AFRL-RD-PS
TP-2010-1017

SYNTHETIC APERTURE IMAGING POLARIMETER: POSTPRINT

Michael R. Roche et al.

Polaris Sensor Technologies
200 West Side Square, Suite 320
Huntsville, AL 35801

1 February 2010

Technical Paper

AIR FORCE RESEARCH LABORATORY
Directed Energy Directorate
3550 Aberdeen Ave SE
AIR FORCE MATERIEL COMMAND
KIRTLAND AIR FORCE BASE, NM 87117-5776

REPORT DOCUMENTATION PAGE

Form Approved
OMB No. 0704-0188

1. REPORT DATE *(DD-MM-YYYY)*	2. REPORT TYPE	3. DATES COVERED *(From - To)*
01/02/2010	Technical Paper	Feb 23, 2007 - Feb 1, 2010

4. TITLE AND SUBTITLE

Synthetic Aperture Imaging Polarimeter: Postprint

5a. CONTRACT NUMBER
FA9451-07-C-0034 DF701826

5b. GRANT NUMBER

5c. PROGRAM ELEMENT NUMBER
65502F

6. AUTHOR(S)

Michael E. Roche*, David B. Chenault*, Justin P. Vaden*, Art Lompado*,
David G. Voelz**, Timothy J.Schulz***,
Ryan N. Givens, Victor L. Gamiz

5d. PROJECT NUMBER
3005

5e. TASK NUMBER
DP

5f. WORK UNIT NUMBER
KA

7. PERFORMING ORGANIZATION NAME(S) AND ADDRESS(ES)

*Polaris Sensor Technologies	**New Mexico State University	***Michigan Technology University
200 West Side Sq, Suite 320	ECE Dept. P.O Box 30001	ECE Dept. 1400 Townsend Dr.
Huntsville, AL 35801	Las Cruces, NM 88003-8001	Houghton, MI

8. PERFORMING ORGANIZATION REPORT NUMBER

9. SPONSORING / MONITORING AGENCY NAME(S) AND ADDRESS(ES)

Air Force Research Laboratory
3550 Aberdeen Ave SE
Kirtland AFB, NM 87117-5776

10. SPONSOR/MONITOR'S ACRONYM(S)
AFRL/RDSE

11. SPONSOR/MONITOR'S REPORT NUMBER(S)
AFRL-RD-PS-TP-2010-1017

12. DISTRIBUTION / AVAILABILITY STATEMENT

Approved for public release

13. SUPPLEMENTARY NOTES
Accepted for publication at the SPIE Conference; Orlando, FL; April 5-9, 2010. 377ABW-2010-0460; March 23,2010. "Government Purpose Rights"

14. ABSTRACT
There is a strong need for the ability to terrestrially image satellites, resident space objects (RSOs), and other low earth orbit (LEO) objects for Space Situational Awareness (SSA) applications. The Synthetic Aperture Imaging Polarimeter (SAIP) investigates an alternative means for imaging and object in LEO illuminated by laser radiation. A prototypw array consisting of 36 divisions of amplitude polarimeters was built and tested. The design, assembly procedure, calibration data and test results are presented. All 36 polarimeters were calibrated to a high degree of accuracy. Pupil plane imaging tests were performed in by using cross-correlation image reconstruction algorithm to determine the prototype functionality.

15. SUBJECT TERMS
Polarimetric Imaging, Division of Amplitude Polarimeter, Imaging Correlography, Pupil Plane Imaging

16. SECURITY CLASSIFICATION OF:			17. LIMITATION OF ABSTRACT	18. NUMBER OF PAGES	19a. NAME OF RESPONSIBLE PERSON Ryan Givens
a. REPORT	b. ABSTRACT	c. THIS PAGE			19b. TELEPHONE NUMBER *(include area code)*
Unclassified	Unclassified	Unclassified	SAR	18	505-846-1947

Standard Form 298 (Rev. 8-98)
Prescribed by ANSI Std. 239.18

THIS PAGE INTENTIALLY LEFT BLANK

Synthetic Aperture Imaging Polarimeter

Michael E. Roche[a], David B. Chenault[a], Justin P. Vaden[a], Art Lompado[a]
David G. Voelz[b], Timothy J. Schulz[c], Ryan N. Givens[d], Victor L. Gamiz[d]
[a]Polaris Sensor Technologies, 200 West Side Square, Suite 320, Huntsville, AL USA 35801;
[b]New Mexico State University, ECE Dept., P.O. Box 30001, Las Cruces, NM88003-8001
[c]Michigan Technological University, ECE Dept., 1400 Townsend Dr, Houghton, MI
[d]AFRL/DE, 3550 Aberdeen Ave SE, Kirtland Air Force Base, NM 87117-5776

ABSTRACT

There is a strong need for the ability to terrestrially image satellites, resident space objects (RSOs), and other low earth orbit (LEO) objects for Space Situational Awareness (SSA) applications. The Synthetic Aperture Imaging Polarimeter (SAIP) investigates an alternative means for imaging an object in LEO illuminated by laser radiation. A prototype array consisting of 36 division of amplitude polarimeters was built and tested. The design, assembly procedure, calibration data and test results are presented. All 36 polarimeters were calibrated to a high degree of accuracy. Pupil plane imaging tests were performed in by using cross-correlation image reconstruction algorithm to determine the prototype functionality.

Keywords: Polarimetric imaging, division of amplitude polarimeter, imaging correlography, pupil plane imaging

1. INTRODUCTION

1.1 Background

A strong need exists to terrestrially image satellites, resident space objects (RSOs), and other low earth orbit (LEO) objects for Space Situational Awareness (SSA), national security, and NASA Safety of Flight applications. A number of image recovery techniques based on active (laser) illumination have been developed over the years to perform this type of imaging, several of which have shown promising results.

The ability to form high resolution images of RSOs through conventional telescope optics is limited mainly by atmospheric turbulence. When light reflected from a point on the RSO propagates through the atmosphere to multiple points across an imager's aperture, they accumulate different amounts of phase (generating wave front error) due to atmospheric turbulence and do not constructively interfere at the image plane. The Airy pattern is significantly blurred, reducing the image fidelity[i]. Current systems utilize highly complex, expensive adaptive optics systems in conjunction with a large aperture telescope to attack this problem. The cost associated with this approach makes it impractical for many applications requiring lower cost solutions. High resolution imaging techniques that do not rely upon adaptive optics systems have numerous applications in surveillance, astronomy and commercial sectors. During the 1990s, significant research was performed by AFRL Directed Energy Directorate on the Active Imaging Testbed program[ii]. The goal of this program was to create an image of satellites in LEO by analyzing the speckle pattern returned through laser illumination. A frequency doubled, Nd:Glass laser outputting 527-nm developed by Lawrence Livermore National Lab (LLNL) was used to illuminate the target in LEO. The reflected energy from the satellite was collected by the 3.5 meter telescope at the Starfire Optical Range (SOR) at Kirtland Air Force Base. The returned speckle pattern was processed using novel polarization-based image reconstruction techniques. The imaging results accomplished in the AIT program prompted the need for further research into a method to provide polarization based imaging, without the need for highly precise, large aperture telescopes.

The effort summarized herein investigates the feasibility of constructing a large-scale sensor, termed the Synthetic Aperture Imaging Polarimeter (SAIP) for measurements of LEO objects. Previous efforts have used large scale telescopes as the collecting aperture. This concept uses a large array of individual polarimeters to collect the returned

energy. The full Stokes vector is measured at each polarimeter. This information is then input into image correlography algorithms that compute auto- and cross-correlation functions of the scattered illumination. In this manner, high resolution RSO images are extracted that are largely immune to atmospheric turbulence effects[iii,iv,v]. **Figure 1** highlights the system concept.

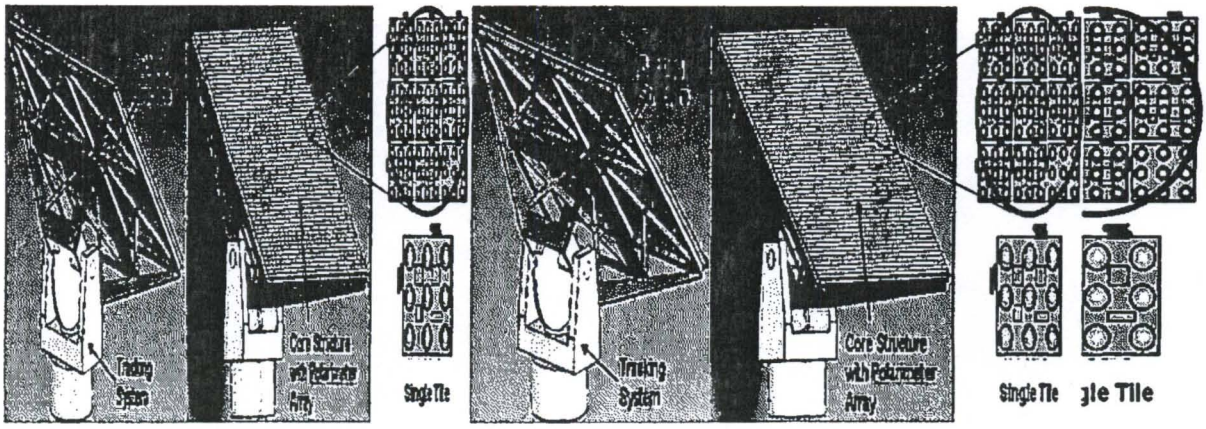

Figure 1. Full scale Synthetic Aperture Imaging (SAIP) concept.

In order to image typical objects (~10 m in size) in low earth orbit (altitudes of approximately 1 x 10^6 m) with laser illumination of 1064 nm, apertures of 10 – 30 m are required. A sensor array of this scale results in tens of thousands of individual polarimeters.

1.2 Polarization-Based Active Imaging Overview

Figure 2 is a diagram of a laser illumination concept for imaging space objects from the ground. The target is illuminated by a polarized laser beam and the reflected light can be considered to consist of two orthogonally polarized components ($\hat{x}$ and $\hat{y}$ for example). In general, the field that results from single surface reflections at the target will be different than the orthogonally polarized component, which requires some multiply surface scatter or volumetric scatter at the target to be created. Assuming the materials that cause single surface reflection and those that cause multiple/volumetric scatter are different then the two fields are associated with two different target reflectivity functions. The two orthogonally polarized fields return through the atmosphere but ideally pick up the same spatial phase aberration ϕ_{atm}. The spatial part of the field components at the receiver can be written as shown in the following equations.

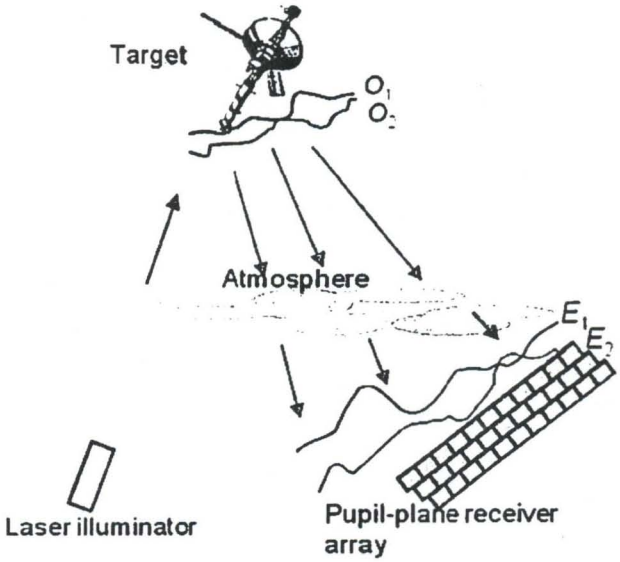

Figure 2. Turbulence canceling laser imaging system concept.

$$E_1(x,y) = A_1(x,y)\exp\left(j\left(\phi_1(x,y)+\phi_{atm}(x,y)\right)\right)\hat{x}$$
$$E_2(x,y) = A_2(x,y)\exp\left(j\left(\phi_2(x,y)+\phi_{atm}(x,y)\right)\right)\hat{y}$$

If one or both fields E_1 and E_2 can be measured by the receiver with the atmospheric phase removed, and the receiver is essentially in the far-field of the reflected pattern, then a 2-D spatial Fourier transform can be performed to estimate the field at the target and thus get an image. For example, if $O_1(x,y)$ is the $\hat{x}$ field reflected at the target and $O_2(x,y)$ is the target $\hat{y}$ field then

$$O_1(x,y) \propto F\{A_1(x,y)\exp(j\phi_1(x,y))\}$$
$$O_2(x,y) \propto F\{A_2(x,y)\exp(j\phi_2(x,y))\} \quad (1\text{-}2)$$

If O_1 and O_2 can be recovered than the intensity images (images of the two target reflectivity functions) are the squared-magnitude of these fields. Unfortunately, getting a measure of the individual phase functions $\phi_1(x,y)$ and $\phi_2(x,y)$ without the atmospheric phase contribution is not straightforward. Suppose a polarimeter with spatial resolution (an array of polarization sensitive subapertures) collects the returning fields. Assuming the correspondence between the polarimeter axis and the $\hat{x}$ and $\hat{y}$ field directions is known, then the following Stokes parameters can be recovered

$$\begin{aligned} S_0(x,y) &= A_1(x,y)^2 + A_2(x,y)^2 \\ S_1(x,y) &= A_1(x,y)^2 - A_2(x,y)^2 \\ S_2(x,y) &= 2A_1(x,y)A_2(x,y)\cos(\phi_1(x,y) - \phi_2(x,y)) \\ S_3(x,y) &= 2A_1(x,y)A_2(x,y)\sin(\phi_1(x,y) - \phi_2(x,y)) \end{aligned} \quad (3\text{-}6)$$

and the following quantities can be found

$$\begin{aligned} A_1(x,y)^2 &= \frac{S_0(x,y) + S_1(x,y)}{2} \\ A_2(x,y)^2 &= \frac{S_0(x,y) - S_1(x,y)}{2} \\ \phi_1(x,y) - \phi_2(x,y) &= \tan^{-1}\left(\frac{S_3(x,y)}{S_2(x,y)}\right) \end{aligned} \quad (7\text{-}10)$$

$A_1(x,y)^2$ and $A_2(x,y)^2$ are the intensities of the returning fields. The atmospheric turbulence phase has been canceled from the measurement, but only a phase difference function is available rather than the individual phase functions. Thus, an estimation approach is needed to find the images from $A_1(x,y)$ and $A_2(x,y)$, and $\phi_1(x,y)$-$\phi_2(x,y)$.

Schulz and Voelz have proposed a method for recovering images with this type of amplitude and phase difference data[v]. Summarizing the approach for a laser imaging system:

1. Assume multiple measurements from a sequence of coherent laser pulses. The multiple pulses are need for averaging speckle noise.
2. Measurements required in the receiver plane for each laser pulse are:
    a. Intensities for each reflectivity function
    b. Coherent phase difference between the two fields corresponding to each reflectivity function
3. Auto- and cross-correlation estimates of the reflectivity functions are produced from the 2-D Fourier transform and averaging of multiple speckle realizations (from the multiple laser pulses).
4. Images (object reflectivity functions) are recovered, using EM recovery algorithm from correlation estimates.

2. PROTOTYPE DESIGN

2.1 Unit Cell Optics Design

A full Stokes vector, division of amplitude design was required to perform polarization-based pupil plane imaging. The circular component of the Stokes vector provides the critical phase information for the cross-correlation algorithm to reconstruct the image. The division of amplitude aspect of the design ensures that the speckle is sampled accurately. The polarimeter provides an average Stokes vector over the aperture of each individual polarimeter. A division of aperture design could produce erroneous values because of the non-uniformity inherent in a speckle pattern. The FOV of the assembly is 0.7° ensuring that the instrument does not sample too large of a portion of the sky; thereby increasing the optical noise in the measurement. The aperture of the design was determined by the 10-cm speckle size determined from the AIT report[ii]. A Nyquist frequency of 2.2 polarimeters/speckle is required to accurately sample the speckle pattern. Therefore, 10-cm divided by 2.2 equals 4.5-cm center to center polarimeter spacing. The size of the collecting aperture was maximized.

An etched diffractive element splits the beam into four equal components. A NIR achromatic doublet then focuses these four fields to the analyzing elements. The analyzing elements consist of a 1064-bandpass filter, followed by the polarizer and retarder elements. The final element in the optical train is the detector. The details of the individual components follow. **Figure 3** highlights the unit cell polarimeter design layout. ZEMAX optical design software was utilized for the optical design and analysis.

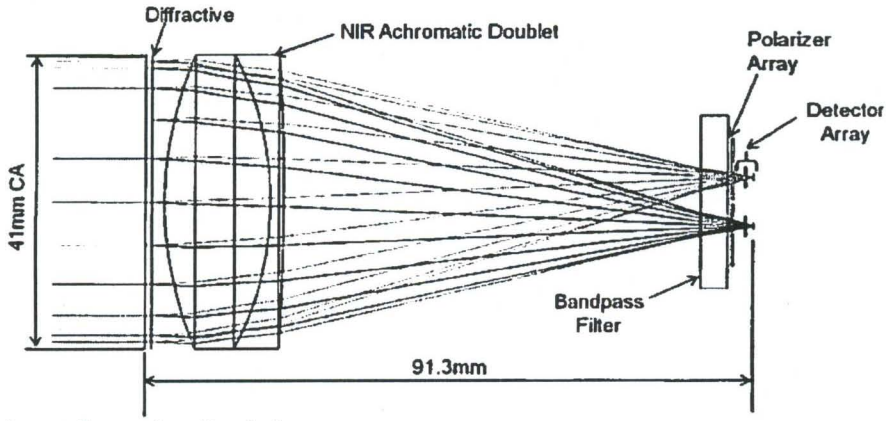

Figure 3. Optics layout for a unit cell polarimeter.

The most critical and most expensive component in the optical train is the diffractive element. The diffractive element divides the beam into four equal components at a prescribed angle, as defined in the optical ray trace. The diffractive element is an etched fused silica wafer produced by Tessera. The efficiency of the diffractive was quoted at 85%. In other words, 85% of collimated light incident on the front surface of the diffractive is split in the prescribed angles. Most of the remained 15% goes into the first order, on axis mode. A small percentage of light goes to higher order modes. After the diffractive element, a NIR achromatic doublet focuses the four branches of light onto their corresponding detectors.

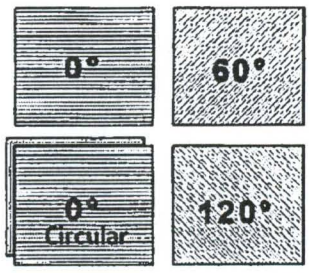

Figure 4. Layout of analyzer elements.

The operational wavelength of the SAIP prototype is 1064-nm. To filter the undesired wavelengths, a bandpass filter must be placed into the optical train. However, the design mandates that off-axis rays will be incident upon the filter, as illustrated in **Figure 3**. A custom filter had to be designed that would maintain narrow bandpass performance while allowing off-axis 1064-nm radiation to pass. The spectral filter performance is slightly reduced due to the converging nature of the incoming beam. The spectral filter has a transmission performance of 94% for rays that have a normal

angle of incidence. Whereas rays at the greatest incident angle of 14°, will be transmitted with 85% efficiency. This slight variation in efficiency will negligibly affect the system performance.

The linear polarizers sample the incoming wavefront at the following orientations: 0°, 60°, and 120°. These three components provide sufficient information to calculate the S_0, S_1 and S_2 components of the Stokes vector. A fourth channel with a 0° polarizer and a ¼ wave retarder is used to measure the S_3 or circularly polarized component of the wavefront. **Figure 4** shows the final layout of the analyzer elements. The detector chosen was the Hamamatsu S2386-18K silicon photodiode. This detector has been used previously with success on other high sensitivity polarimeters built by Polaris. The detector is a highly sensitive, low noise photodiode that operates from the visible spectrum to approximately 1100-nm.

ZEMAX optical design software was used to design the optics train. Mechanical and optical tolerances were input to ensure a robust design. The goal of the design was to be able to assemble each polarimeter and not require active alignment. This feature is critical in the full scale concept, comprised of thousands of individual polarimeter. This goal was accomplished. **Figure 5** shows the geometric spot size and location relative to the detector surface, including the stackup of optical and mechanical tolerances.

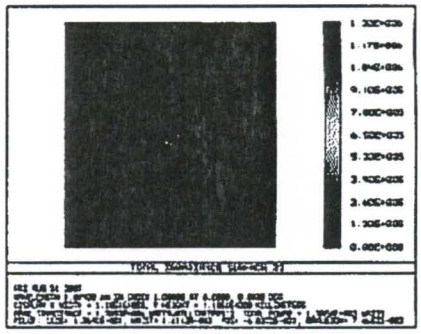

Figure 5. Spot size relative to detector surface.

2.2 Modular Assembly

The mechanical design of the SAIP prototype revolves around the concept of a modular array. The modular aspect allows for the array to be built in tiles and then assembled onto the large scale platform. Each tile can be serviced or replaced by removing the tile from the assembly and replacing either with a new tile or after fixing any problems. In the Phase II SAIP prototype, a 2x2 tile of polarimeters is used to prove the modular concept. However, it is envisioned that on the full scale design, the tiles would be comprised of more elements. Figure 6 shows the tile concept, highlighting the components of an individual tile.

Nine tiles comprise the 6x6, 36 polarimeter SAIP prototype array. These tiles mount to a common, precision machined frame. This frame maintains angular alignment between tiles through a precision ground surface. Each tile is held in place with two screws and two dowel pins provide x-y alignment. **Figure 7** highlights the tiled array comprising the 356 channel SAIP prototype.

Each of the tile assemblies contains a custom electronics assembly that consists of an analog amplifier card and an analog-to-digital (ADC) card.

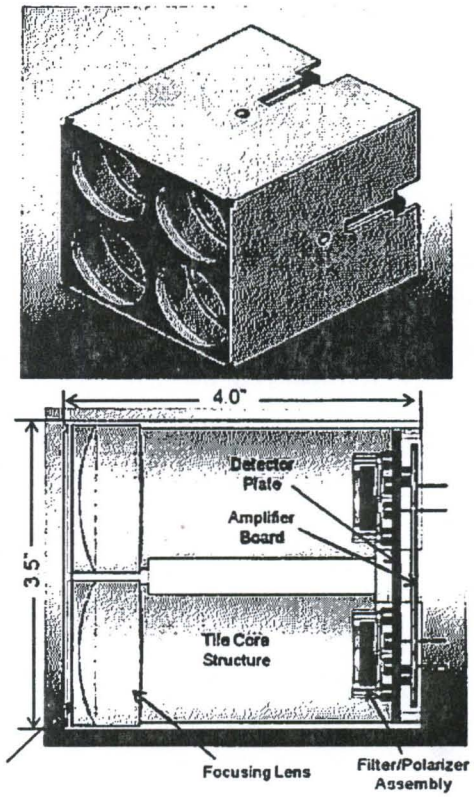

Figure 6. Individual tile assembly.

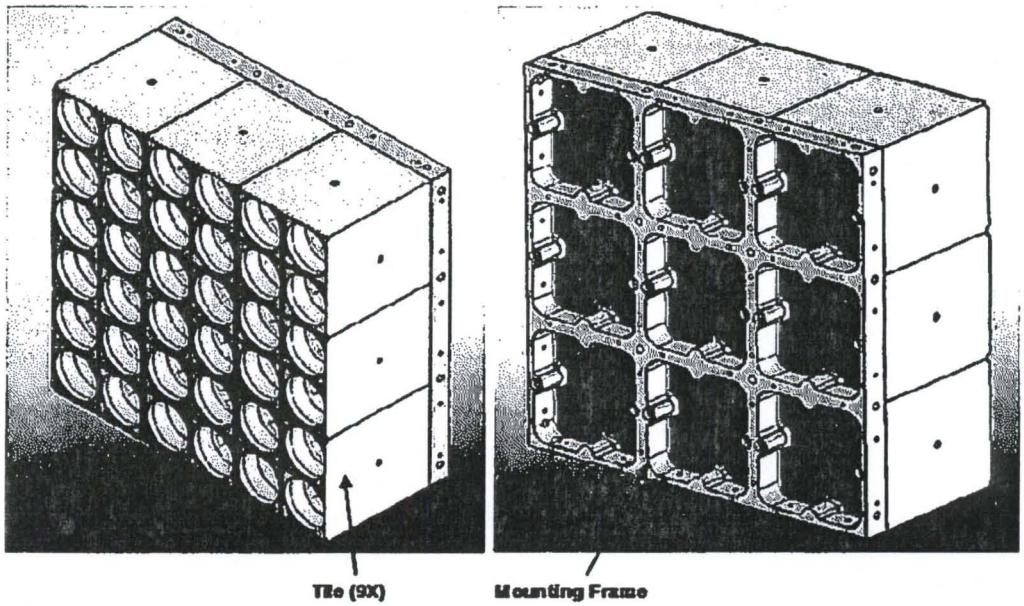

Figure 7. Nine tiles mounted to high precision mounting frame, completed SAIP prototype.

2.3 Electronics

Three separate custom circuit card designs were required on this effort: analog amplifier PCB, analog-to-digital converter (ADC) PCB and an interconnect PCB. **Figure 8** shows a connectivity diagram for the electronics system.

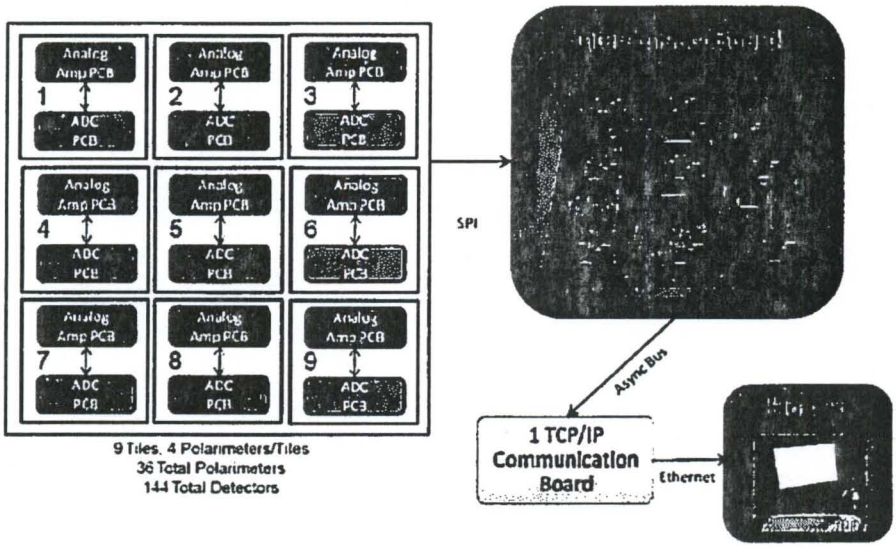

Figure 8. Electronics connectivity diagram.

The analog amplifier PCBs contain the silicon photodiodes and their accompanying two-stage amplifier. The two stage design allows for a high gain while minimizing noise. Each tile contains an analog amplifier PCB and an ADC. Each tile consists of four complete polarimeters. The analog amplifier PCB is soldered to the detector leads, the ADC PCB mounts to the analog amplifier PCB via board-to-board connectors and standoffs. The interconnect board bridges the nine analog amplifier/ADC assemblies, providing power and communication between the tiles. A COTS TCP/IP board provides communication to the host PC.

3. CALIBRATION

3.1 Calibration Setup

Figure 9 shows the laboratory arrangement of the calibration setup. The light source is a 20" integrating sphere whose exit aperture is reduced to a 1 mm dimater pinhole. Light from this pseudo-point source is collimated, passes through a calibration polarizer, and into the aperture of a single sensor. The pinhole size and lens focal length are selected to produce spot images that slightly underfill the four detector elements of a single sensor. Alignment of the source beeam to the sensor is very sensitive owing to its small field of view (FOV) of 0.7°. Therefore, once the source was constructed, the polarimeters were moved into the beam sequentially using a kinimatic mount with x-y translation capability.

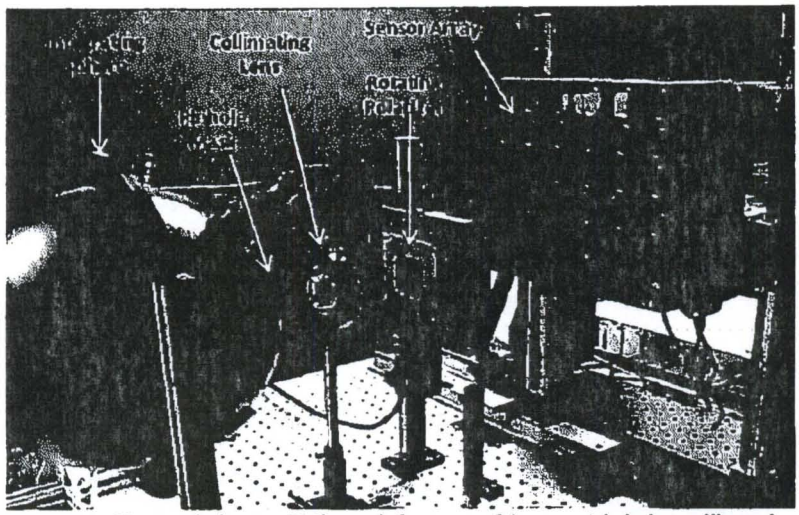

Figure 9. Calibration arrangement. Here, polarimeter #6 (lower left corner of the array) is being calibrated.

3.2 Calibration Procedure and Results

The procedure is initiated by introducing purely unpolarized light into the sensor and first identifying the individual channels' response characteristics for two extreme light levels; the maximum attainable and the case where no light is incident, refferd to as the "high" and "low" measurements respectively. This represents the radiometric part of the calibration and is thus performed without the calibration polarizer in place. The mean value of multiple measurements of each case are made in an effort to reduce the effects of systemic noise (e.g., Shott noise, electronics noise, etc.) on each measurement. We note that the "low" measurements represent the electronic equivalent of the channel biases while the "high" values represent their gains. The biases are subtracted from all subsequent measurements, which are then divided by the gains are used to normalize the responses.

The next phase of calibration consists of measurement of the channel responses for a known set of input polarization states. Generation of the known states is achieved through the introduction of the high quality linear calibration polarizer prior to the sensor aperture. This polarizer can be discretely rotated to serially introduce uniquely oriented linearly polarized inputs. Monitoring the irradiance at each detector over a single rotation of the calibration polarizer (in 1° increments) results in a set of unnormalized calibration modulation curves. These curves are then normalized using their respective "high" and "low" measurements and are displayed in **Figure 10.** Note how the responses for those channels containing only linear polarizers (channels 1, 2, and 4) produce sinusoidal modulations with relatively large amplitudes, a result attributable to Malus' law[vi]. Channel 3, which contains a linear ¼ wave retarder whose axes are oriented at 45° relative to a subsequent linear polarizer, is seen to produce a damped but discernable modulation. In theory, this retarder-polarizer combination produces a circular analyzer and should exhibit no modulation at all for the linearly polarized input states. The fact that channel 3 shows some modulation implies that the polarization elements are nonideal, misaligned, or some combination thereof which causes the observed slight deviation from the theoretical straight line.

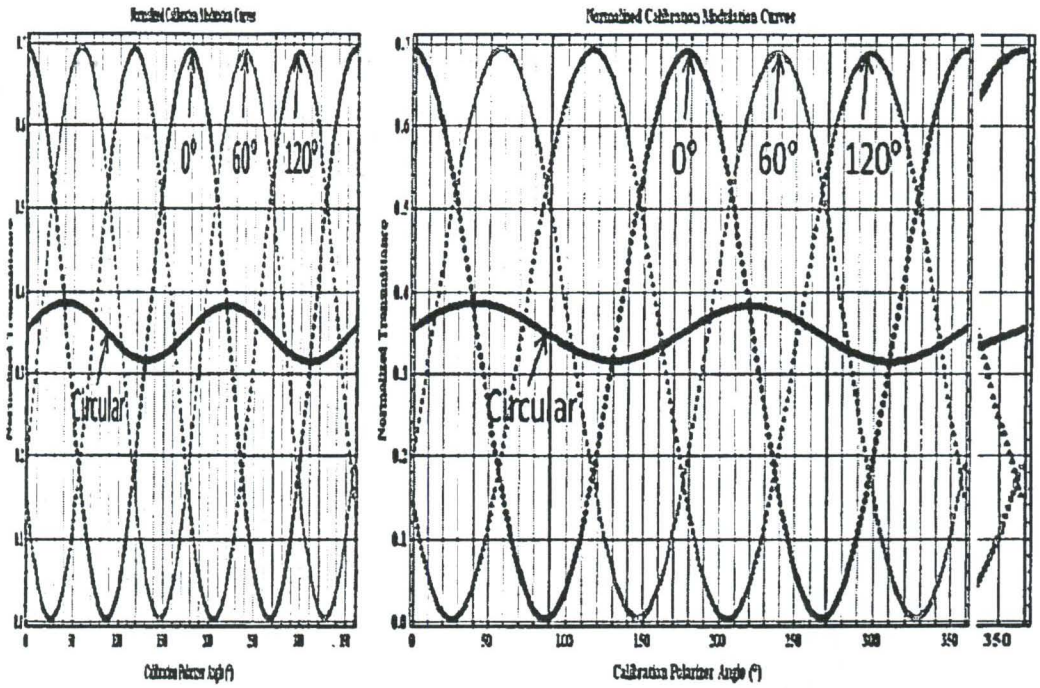

Figure 10. Normalized calibration modulation curves.

The next step in the calibration procedure is to determine the exact principal transmittance values and axes orientations for the polarizers in each channel, in addition to the orientation and retardance of the ¼ wave plate in channel 3. According to the Stokes-Muller polarization calculus, these parameter values may be determined from the measured irradiance at each channel of the sensor according to the following equations.

$$I_1 = \tfrac{1}{2}\left((q_1 + r_1)^2 + (q_1 - r_1)^2 \cos[2(\theta - \phi_1)]\right)$$
$$I_2 = \tfrac{1}{2}\left((q_2 + r_2)^2 - (q_2 - r_2)^2 \sin[2(15° - \theta + \phi_2)]\right)$$
$$I_3 = \tfrac{1}{2}\left((q_3 + r_3)^2 + (q_3 - r_3)^2 \left(\cos[2(\theta_3 - \theta)]\cos[2(\theta_3 - \phi_3])\right] + \cos[\delta]\sin[2(\theta_3 - \theta)]\sin[2(\theta_3 - \phi_3)]\right)\right)$$
$$I_4 = \tfrac{1}{2}\left((q_4 + r_4)^2 + (q_4 - r_4)^2 \cos[2(-120° + \theta - \phi_4)]\right)$$

(11-14)

Here, q_i and r_i ($i = 1 \ldots 4$) are the polarizer principal transmittances and ϕ_i are their axes orientations, θ_3 is the ¼ wave plate orientation and δ is its retardance while θ is the orientation of the calibration polarizer. Acquisition of 360 discrete measurements yields a system of 360 equations containing these 14 unknown parameters. This over specified system of equations is then solved for the unknown parameters through a nonlinear fitting routine based on the Levenburg-Marquardt regression algorithm. The regressed values for the curves of **Figure 10** are given in **Table 1**.

Table 1. Regressed polarization element parameter values.

	q (%)	r (%)	Polarizer Offset	QWP Angle	QWP Retardance
Channel 1	69.19	0.0008	-2.3°		
Channel 2	69.31	0.0013	-2.2°		
Channel 3	69.21	0.0038	1.2°	43.3°	89.48°
Channel 4	69.24	0.0012	-3.5°		

The principal transmittances (i.e., q_i and r_i) were all calculated to be quite close to the expected values of 69.2% and 0.001% for all channels and the ¼ wave plate's retardance is also very close to the ideal values of 90° (Note that the difference amounts to only $360°/0.52° \approx \lambda/692$). Similarly, the polarizer axes' offsets from the target values are within a

few degrees of the expected values (ideally 0°) and the retarder's is seen to be within 2° of the nominal 45° position. The measured offsets can easily be attributable component and to assembly tolerances. Inserting the calculated parameter values into Equations 11-14 above produced extremely accurate fits to the measured data sets. These highly accurate fits imply that the regressed parameters are indeed representative of the physical characteristics of the polarization element(s).within each channel and will thus serve to produce accurate Stokes vector for any subsequent measurements.

Once the fitted parameters have been obtained, the so-called calibration matrix may be constructed[vii]. The inverse of the calibration matrix (presuming it is nonsingular) yields the so-called polarimetric data reduction matrix (DRM). The DRM is a 4x4 matrix through which any subsequent measurements (i.e., the 4 channel irradiances) are processed to yield the four element Stokes vector of the incident light. As a self consistency check, the initial data set (i.e., that acquired to perform the calibration) was next processed using the DRM derived from the regressed parameters. The resulting Stokes vectors were then converted into the conventional derived polarization metrics including the Degree of Polarization (DoP), the Degree of Linear and Circular Polarization (DoLP and DoCP), and the orientation of the linear component of the incident field. Incidentally, the known orientations come from the readings off a motorized stepper motor whose specified accuracy is 0.001°. The results of this check yielded DoP, DoLP and DoCP values well within 0.5% of the known values. Similarly, the orientation error (measured orientation – known orientation) was below 0.1° for all 360 measured orientations

Finally, we note that the self consistency check is just that, a technique to verify that the mathematics behind the calculation of the system's DRM is valid. A more practical characterization of the sensor is a measure of its repeatability. To that end, a second measurement, performed exactly as the calibration, was made to assess each sensor's repeatability. In this case the derived polarization products are calculated from the measured raw data using the DRM obtained from the calibration. **Figure 11** shows the results of this measurement in terms of the measured derived polarization parameters.

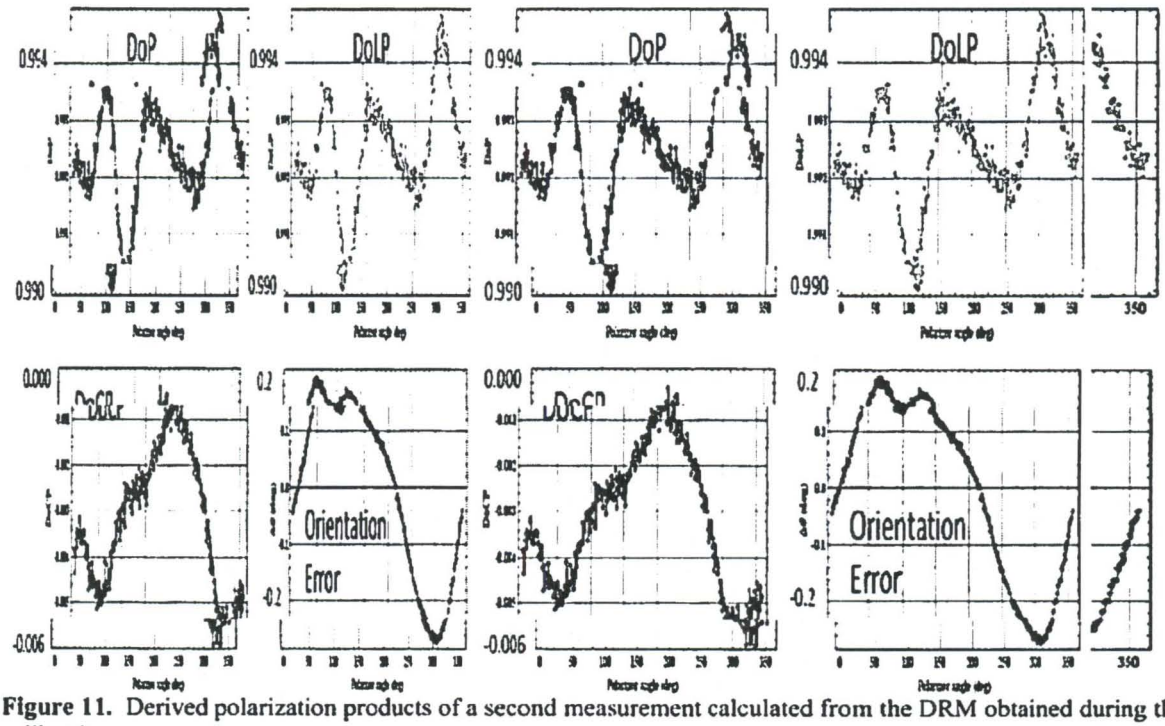

Figure 11. Derived polarization products of a second measurement calculated from the DRM obtained during the calibration.

The figure shows good accuracy and stability across all 360 input states with most of the polarization found to be in the linear component as expected. Do(L)P values of approximately 99.2% are expected from the known principal transmittance values of the measured polarizer and the expected orientation errors of 0° are also found to be very closely approximated. As a final note, we reiterate that the entire procedure described in this section was performed for each component sensor in the 6x6 array of polarimeters, with results practically equivalent to those presented. In fact, the results for this polarimeter may be considered nominal in that they are not substantially better (or worse) that those obtained for the other 35 sensors. **Table 2** shows data for all 36 polarimeters compressed into key parameters.

Table 2. Calibration data averaged for all 36 polarimeters. (I think the formatting rules say this label should be centered over the table)

	DoP (%)	DoLP (%)	DoCP (%)	ΔΘ(°)
Mean	99.166	99.162	-0.321	-0.015
Standard Deviation	0.349	0.345	0.715	0.182

The calibration of all 36 polarimeters in the SAIP prototype showed all the polarimeters to be highly accurate. It is also important to note that they source position was not adjusted to maximize the uniformity on each channel. The source was held stationary, while the array moved in the x and y direction to the prescribed polarimeter. Therefore, the accuracy of the calibration data acts also as a boresighting verification. If the optical axes of each polarimeter were not parallel within the FOV of the sensor, the calibration would not hold across sensors.

4. IMAGING TEST

4.1 Imaging Test Overview

An end-to-end test of the optics, electronics and algorithm was required to prove the validity of the SAIP instrument as an active imaging instrument. The ultimate goal of the concept is to sample a returned speckle pattern from a target object, process the returned light and generate a reconstructed image. Numerous concepts were discussed ranging from laboratory scale experiments to full scale field tests. The field test options were attractive in that the polarimeter array would be tested with a real system. However, it was deemed that too many unknowns were present in the field test alternatives for this early level prototype. The number of unknowns present in the test added risk that could deem the test a failure while still not determining the functionality of the SAIP prototype array. In the end, it was decided that a laboratory scale experiment with a known input would be the best way to prove the concept at this level.

A known interference pattern needed to be created that could 1) be resolved by a 36 channel array and 2) provide both intensity and phase information to the sensor. The algorithm developed by Schulz and Voelz was to be used for the image reconstruction[v]. The algorithm requires both intensity and phase information to reconstruct the original image using a returned speckle pattern. The laboratory scale experiment decided upon uses a novel dual Michelson interferometer concept. Each leg of the Michelson has a unique polarization state created by passing the light through a 50/50 polarizing beamsplitter. The x polarization component is transmitted, while the y polarization component is reflected. Each leg is treated as an individual Michelson interferometer and recombined. By adjusting the fringe spacing and orientation, simple interference patterns consisting of a "checkerboard" style pattern of maximums and minimums can be created. The combined beams are then passed through a microscope objective, which expands the beam to a parabolic mirror. The parabolic mirror collimates and redirects the beam to the sensor array. A diagram of the experimental layout can be seen in **Figure 12.**

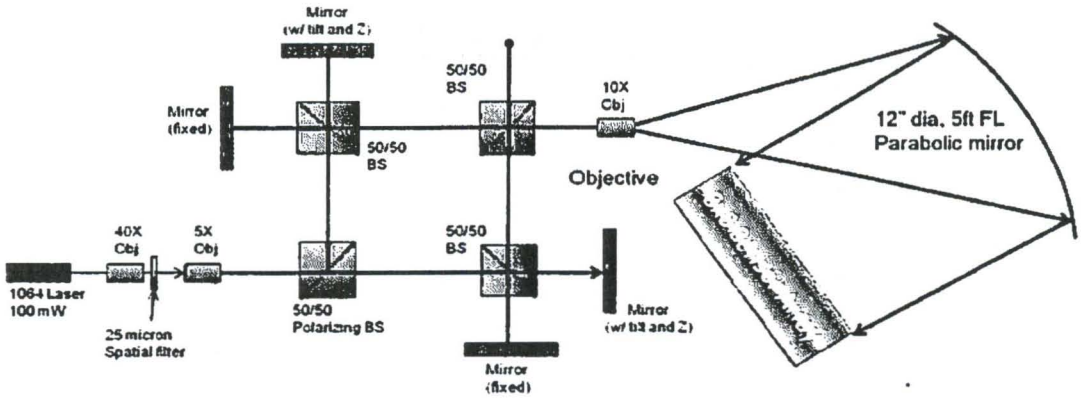

Figure 12. Dual Michelson interferometer used for imaging test.

Simulations were performed to determine how fringe width, spacing and orientation would effect the reconstructed image. **Figure 13** shows an example of a reconstructed image. Theoretically, the algorithm would reconstruct the four original spots that created the fringe pattern. The separation of these spots correlates to the fringe spacing and the orientation of the spots corresponds to the angular orientation of the fringe pattern.

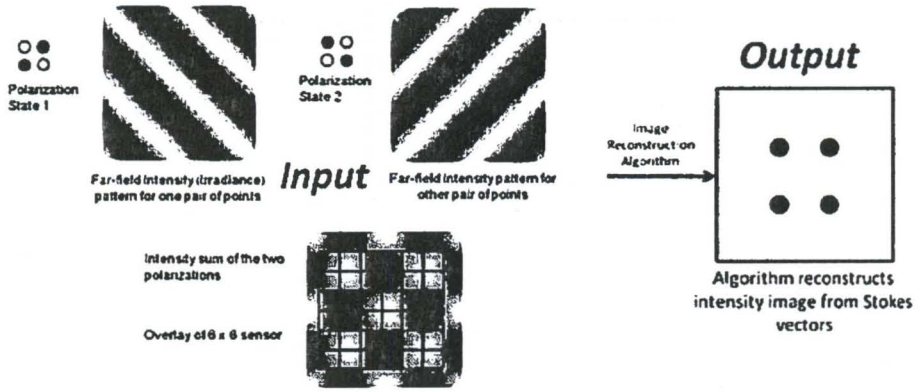

Figure 13. Example of output from dual Michelson interferometer and the final reconstructed image.

The experiment was constructed and data was taken. **Figure 14** shows example results based upon the nominal case of approximately three fringe cycles over the entire array.

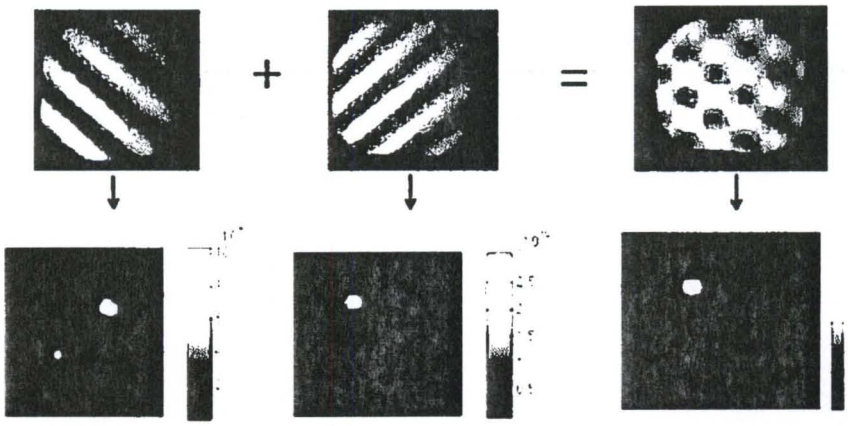

Figure 14. Processed image data. Top row is raw light incident on array. Bottom row is process imagery of source.

The top row images are of the actual fringe pattern incident on the SAIP prototype array. These pictures were taken through the handheld IR viewer with a digital camera. The individual component fringes of the x polarization component field (45° fringe orientation) and the y polarization component field (135° fringe orientation) were captured by blocking the other branch of the dual Michelson. The bottom row shows the processed images associated with each of the inputs.

The results demonstrated that the SAIP prototype array works in conjunction with the algorithm developed by Schulz. Starting with a checkerboard interference pattern, the four unique beams of the dual Michelson interferometer were reconstructed using intensity and phase information garnered through the 6x6 polarimeter array. This method follows the logic used on the AIT effort[ii]. In addition, the pairs of spots were seen to rotate with the change in orientation of the corresponding component fringe pattern. Varying intensity was also noticed in each spot, correlating to the intensity of the corresponding beam.

5. CONCLUSIONS

The goal of this effort was to design, fabricate and test a polarimeter array capable of being used in polarization-based active imaging concepts. The foundation of this effort was the AIT performed at AFRL Kirtland during the 1990s. A modular design comprised of 9 tiles, each containing a 2x2 array of polarimeters, totaling 36 polarimeters was constructed. Each polarimeter was a division of amplitude, full Stokes design. The baseline design for the array uses a CW laser source for laboratory experimentation purposes. However, a full electronics design effort was also completed demonstrating its ability to operate with a pulsed laser source.

The array was calibrated and tested thoroughly. The calibration results demonstrated the array to be highly accurately. The average polarization product data over all 36 polarimeters shows that the degree of polarization to be 0.349% with an orientation accuracy of 0.182°. The calibration test also verified the boresight accuracy of the array. Each polarimeter has a 0.7° FOV. The source was held stationary while the array was translated on linear rails in the x and y direction to the desired polarimeter. If the there were angular errors in the assembly, they would manifest by showing non-uniformities between polarimeters. However, this was not observed. The uniformity between polarimetric measurements was excellent.

An imaging test was devised to simulate a simple speckle pattern by creating a known interference pattern at the surface of the array. A polarized, dual Michelson setup was determined to be the best laboratory scale experiment as the proof of concept. A checkerboard interference pattern was placed onto the array. The checkerboard pattern was created using one simple linear fringe pattern of horizontally polarized light interfering with another simple linear fringe pattern of vertically polarized light, with the two interference patterns rotated 90° from each other spatially. Data was collected and processed at the array. The Stokes vector data was then processed with the algorithm developed by Schulz. The processed data yielded an image of the original four spots that comprised the checkerboard interference pattern. This was deemed a success, the SAIP prototype works with the algorithm logic developed on the AIT effort.

REFERENCES

[i] J. W. Hardy, *Adaptive Optics for Astronomical Telescopes*, Oxford University Press (1998).

[ii] AFRL Technical Report, AFRL-DE-TR-2000-1045, Active Imaging Test Bed Final Report, Design and Field Operations Summary, June 2000.

[iii] P.S. Idell, J. R. Fienup, and R.S. Goodman, "Image synthesis from non-imaged laser-speckle patterns," Opt. Lett. **12**, 858-860 (1987).

[iv] J. W. Goodman, "Statistical properties of laser speckle patterns," in *Laser Speckle and Related Phenomena*, J. C. Dainty, ed. (Springer-Verlag, New York, 1975), pp. 9-68.

[v] T. J. Schulz, D. G. Voelz, "Signal recovery from autocorrelation and cross-correlation data," J. Opt. Soc. Am. A, 22, 616-624, (2005).

[vi] Hecht, Eugene, Optics, 2nd Ed, Addison Wesley, 1987

DISTRIBUTION LIST

DTIC/OCP
8725 John J. Kingman Rd, Suite 0944
Ft Belvoir, VA 22060-6218 1 cy

AFRL/RVIL
Kirtland AFB, NM 87117-5776 2 cy

Ryan Givens
Official Record Copy
AFRL/RDSEA 1 cy